RESEARCH ARTICLE

Check for updates

A polar two-dimensional lead-free hybrid perovskite for self-powered polarization-sensitive photodetection†

Cheng-Dong Liu, [ID] Chang-Chun Fan, [ID] Bei-Dou Liang [ID] and Wen Zhang [ID] *

Two-dimensional (2D) lead hybrid perovskites have attracted great attention due to their excellent stability and unique physical and chemical properties. Nevertheless, the toxicity of lead remains an urgent issue. Lead-free homovalent substituents (Sn^{2+} and Ge^{2+}) suffer from poor oxygen-sensitive stability, posing a serious challenge to their device applications. Compared to homovalent substituents, heterovalent substituted perovskites based on the VA group elements, especially bismuth, exhibit excellent stability, making them more competitive. However, 2D Bi-based perovskites with the composition 2D A_2BiX_4 (A = organic cation; X = Cl^-, Br^- or I^-) cannot be formed considering the charge balance. Here, by reducing the occupancy rate of Bi^{3+} ions, we successfully obtained the first polar 2D Bi-based perovskite $(4BrPEA)_3BiI_6$ (4BrPEA = 4-bromophenethylammonium) with an A_2PbX_4-like layered structure. $(4BrPEA)_3BiI_6$ exhibits a narrow bandgap (2.00 eV) and excellent photoelectric response performance. Specifically, a single crystal device based on $(4BrPEA)_3BiI_6$ has been explored for self-powered polarization-sensitive photodetection with a large photocurrent anisotropic ratio ω of 2.16. This work demonstrates the great potential of heterovalent substituted 2D lead-free perovskites and opens up a new way to expand the synthesis of environmentally friendly and high-performance self-powered polar optoelectronic semiconductor materials.

Introduction

Lead-based hybrid perovskites, represented by $CH_3NH_3PbI_3$, have attracted significant attention in various fields, including photovoltaics,[1] light-emitting diodes,[2] photoluminescence,[3] ferroelectricity,[4–6] and photodetection,[7,8] on account of their excellent physical and chemical properties.[9–11] However, their instability and toxicity greatly hinder further commercial development.[12–14] Usually, the stability issues can be effectively addressed by employing dimensional reduction technology to construct 2D hybrid perovskites.[15] 2D perovskites possess excellent chemical stability compared to typical 3D $CH_3NH_3PbI_3$ due to their quantum well structure of hydrophobic organic cations and inorganic perovskite layers. The alternant quantum well structure also introduces natural structural anisotropy for 2D perovskites, which facilitates the realiz-

ation of polarization-sensitive detection.[16–19] In particular, polar 2D perovskites exhibit the bulk photovoltaic effect (BPVE), which can produce stable open-circuit voltage and short-circuit current under illumination, making them candidates for highly efficient self-powered polarization-sensitive photodetectors.[17] Although considerable progress has been made in lead-based 2D perovskite self-powered polarization-sensitive photodetection, the toxicity of lead remains a pressing issue.

Lead-free is the development trend of green chemistry in perovskites. To obtain 2D lead-free hybrid perovskites, two strategies have been developed: homovalent substitution and heterovalent substitution. Although Group IVA homovalent substituent (Sn^{2+} and Ge^{2+}) perovskites have produced decent optical and electrical properties, their poorer oxygen-sensitive stability than lead-based perovskites poses a serious challenge to their device applications.[12] Compared to homovalent substitution, heterovalent substitution based on the VA group element bismuth is more competitive. Bi^{3+} has the same $6S^2 6P^0$ external electron configuration and a similar ionic radius to Pb^{2+}, and its stability and semiconductor properties have been widely demonstrated.[14] However, due to the total charge δ of the composition A_2BiX_4 (A = organic cation; X = Cl^-, Br^- or I^-) greater than 0, the typical (100)-oriented 2D

This journal is © the Partner Organisations 2024

Inorg. Chem. Front., 2024, **11**, 4611–4618 | **4611**

layered perovskites cannot be formed. Thus Bi-based hybrid perovskites tend to form low-dimensional 0D or 1D structures (*e.g.* 0D $A_3Bi_2X_9$, 0D A_3BiBr_6, 1D $ABiX_4$, and 1D A_2BiX_5).[20–24] To satisfy the total charge balance and to form 2D A_2PbX_4-like structures simultaneously, it is necessary to reduce the occupancy of Bi sites (*i.e.*, by introducing vacancies on the metal sites) on the layer. By reducing the chemical occupancy of Bi sites from 1 to 2/3, stable (100)-oriented 2D perovskites with the composition A_3BiX_6 can be formed (Scheme 1). Obviously, that is difficult in synthesis because the inherent driving force to form other non-vacancy structures cannot be avoided. At present, a 2D Bi-based perovskite is still a type of under-explored material with only three examples reported, all of which are non-polar structures.[25–27] Polar perovskite materials, including ferroelectrics and pyroelectrics, have emerged as competitive self-powered photodetection candidates.[7,17] In this context, it is urgent to develop polar Bi-based perovskites for green and high-performance self-powered polarization-sensitive photodetection.
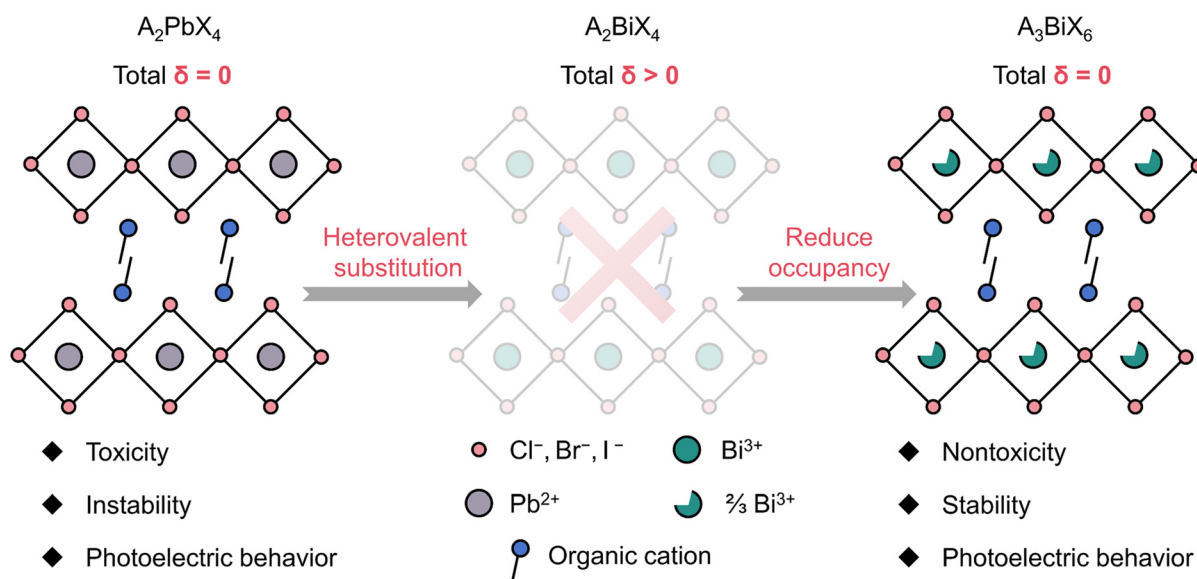
Organic cations were shown to have the potential to template unusual hybrid perovskite structures,[15] especially the halogenated organic cations that have the potential to control crystal symmetry breaking.[28] Herein, we report the first polar 2D lead-free perovskite $(4BrPEA)_3BiI_6$ (4BrPEA = 4-bromophenethylammonium). $(4BrPEA)_3BiI_6$ possesses an A_2PbX_4-like layered structure, where the occupancy rate of Bi atoms on the 2D layer is 2/3. The directional effect of brominated organic cations on polar structures was demonstrated through single crystal structure analysis. $(4BrPEA)_3BiI_6$ exhibits excellent semiconductor performance with a narrow bandgap of 2.00 eV. Benefiting from the polar structure, polarization-sensitive detection devices based on $(4BrPEA)_3BiI_6$ exhibit a large anisotropy factor ω of 2.16, which is comparable to that of Pb-based perovskites.

Results and discussion

Crystal structure analysis

Dark red single crystals of $(4BrPEA)_3BiI_6$ were obtained by the slow temperature cooling method (Fig. S1, ESI†). The powder X-ray diffraction (PXRD) pattern of the powder sample matches well with the simulated results (Fig. S2, ESI†), which verifies the phase purity of the as-synthesized crystal. The PXRD spectrum of the single crystal shows the signals of the $(0k0)$ plane. The thermogravimetric analysis shows that $(4BrPEA)_3BiI_6$ has good thermal stability up to 500 K (Fig. S3, ESI†). Single crystal X-ray diffraction (SC-XRD) shows that $(4BrPEA)_3BiI_6$ crystallizes in the polar space group *Fmm*2 (No. 42). Other crystal data and structure refinement details, bond lengths, and bond angles are presented in Tables S1, S2, and S3 in the ESI,† respectively. Crystal structure analysis reveals that the organic cation 4BrPEA separates the inorganic octahedral layer $[BiI_6]^{3-}$ along the b-axis to form a typical (110)-oriented 2D quantum well structure (Fig. 1a). The I2A and I2B in the asymmetric unit were refined to be disordered, and their chemical occupancy was freely refined to 0.657 and 0.343 (Fig. S4, ESI†). Specifically, the chemical occupancy of Bi sites was fixed at 2/3 to meet the charge balance. Finally, the formula of $(4BrPEA)_3BiI_6$ was adopted, and the total charge δ was kept at 0.

In $(4BrPEA)_3BiI_6$, the 2D layer is constructed by corner-sharing $Bi_{2/3}I_6$ octahedra, and the 4BrPEA cations and $Bi_{2/3}I_6$ octahedra are ordered along the c-axis, which results in a polar structure. The second harmonic generation signal obtained at room temperature verifies the polar structure (Fig. 1b). It is worth noting that $(4BrPEA)_3BiI_6$ is the first polar 2D Bi-based hybrid perovskite. By comparing with the reported 2D centro-symmetric structure of $(4FPEA)_3BiI_6$ (its space group is $C2/c$; 4FPEA = 4-fluorophenethylammonium),[26] the origin of electri-

Scheme 1 The strategy of forming the 2D Bi-based perovskite structure. δ represents the total charge.

4612 | *Inorg. Chem. Front.*, 2024, **11**, 4611–4618
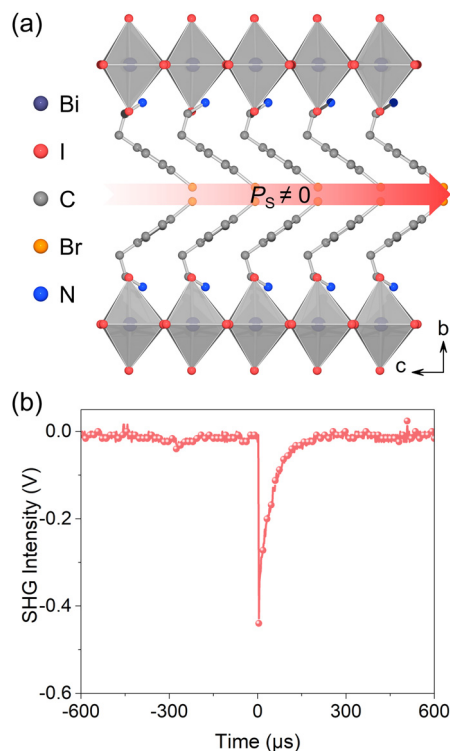
This journal is © the Partner Organisations 2024

Fig. 1 (a) 2D polar structure of $(4BrPEA)_3BiI_6$ viewed along the *a*-axis. (b) The second harmonic generation signals of $(4BrPEA)_3BiI_6$.

Fig. 2 (a) Crystal structure of $(4FPEA)_3BiI_6$ viewed along the *b*-axis. (b) C−F⋯π interactions in $(4FPEA)_3BiI_6$. (c) Crystal structure of $(4BrPEA)_3BiI_6$ viewed along the *c*-axis. (d) C−Br⋯π interactions in $(4BrPEA)_3BiI_6$.

cal polarization of $(4BrPEA)_3BiI_6$ was analyzed. $(4BrPEA)_3BiI_6$ and $(4FPEA)_3BiI_6$ are composed of similar organic cations, with the only difference being the halogen species on the *para*-position of the benzene ring. In $(4FPEA)_3BiI_6$, the 4FPEA cations exhibit an edge-to-face parallel arrangement with C−F⋯π interaction distances ranging from 3.713 to 3.830 Å (Fig. 2a and b). While in $(4BrPEA)_3BiI_6$, the orientation of the 4BrPEA cations exhibits vertical arrangement to adapt to strong C−Br⋯π interactions (3.417–3.424 Å) (Fig. 2c and d). In $(4BrPEA)_3BiI_6$ and $(4FPEA)_3BiI_6$, the main interaction between the $[BiI_6]^{3-}$ layer and the organic amine cations is the N−H⋯I hydrogen bond, and the bond length range is roughly the same (Table S4, ESI†). Therefore, in $(4BrPEA)_3BiI_6$, the strong C−Br⋯π interactions drive the orientation arrangement of cations within the organic layer, which leads to the separation of positive and negative charges along the *c*-axis and ultimately results in the polar structure.[28]

Semiconductor and optoelectronic properties

2D lead-free hybrid perovskites based on bismuth are expected to exhibit semiconducting-related optoelectronic behavior comparable to those of lead-based compounds. To character-ize the semiconducting properties of $(4BrPEA)_3BiI_6$, ultraviolet-visible (UV-vis) absorption spectra were recorded. As shown in Fig. 3, $(4BrPEA)_3BiI_6$ exhibits an absorption cutoff of around 670 nm and a bandgap of 2.00 eV derived from the Kubelka–Munk function. Compared with the reported 2D Pb-based hybrid perovskites, such as $(4BrPEA)_2PbI_4$,[29] $(4AMP)PbI_4$

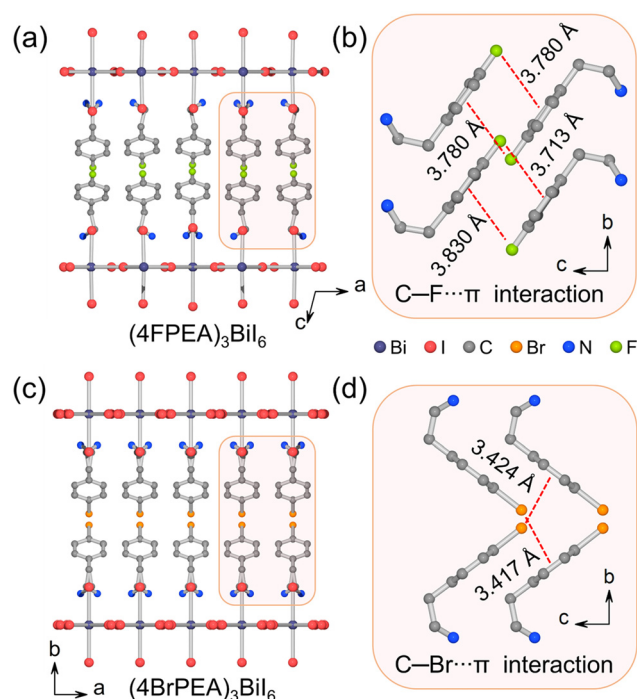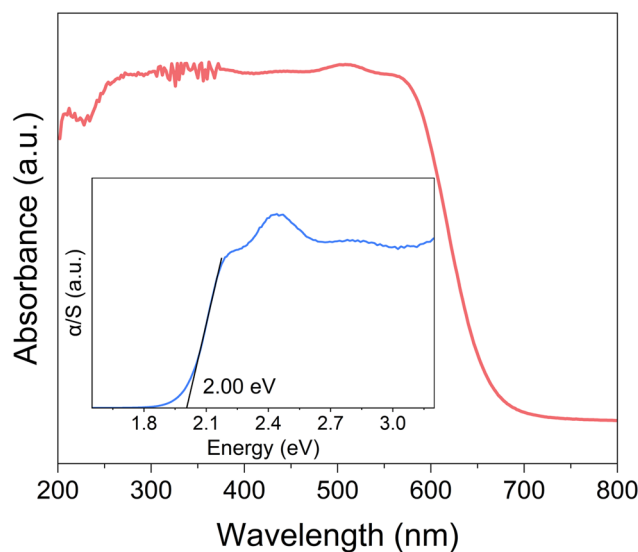**Fig. 3** UV-vis absorption spectra of $(4BrPEA)_3BiI_6$. Insert: the optical bandgap.

$(4AMP = 4\text{-(aminomethyl)piperidinium})$,[30] and $(BA)_2PbI_4$ (BA = *n*-butylammonium),[31] 2D lead-free Bi-based perovskites exhibit a smaller bandgap.

Band gap analysis shows that $(4BrPEA)_3BiI_6$ has the poten-tial to be an optoelectronic material.[14,32–34] Therefore, we further investigated its photoresponse behavior upon 405 nm LED light irradiation under a 10 V bias. Fig. 4a shows the

This journal is © the Partner Organisations 2024

Inorg. Chem. Front., 2024, **11**, 4611–4618 | **4613**

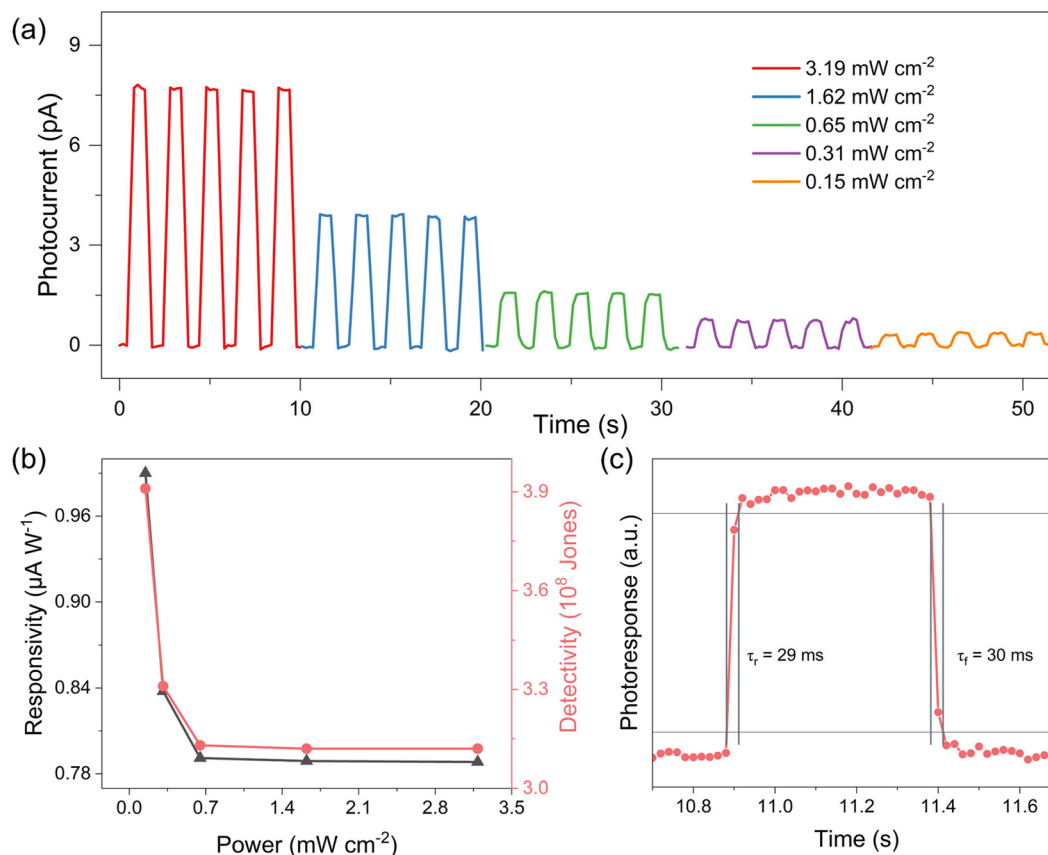**Fig. 4** (a) The I–t curve of the $(4BrPEA)_3BiI_6$ single crystal device at 405 nm under 10 V bias. (b) The calculated R and D^* related to the optical density. (c) The rise and decay time.

time-dependent photocurrent (I–t) of the $(4BrPEA)_3BiI_6$ single crystal device at different optical power densities. The photocurrent reaches 7.6 pA under an optical power P of 3.19 mW cm^{-2}, and the corresponding I_{ph}/I_{dark} ratio is 10^2. Even under an optical power of 0.15 mW cm^{-2}, $(4BrPEA)_3BiI_6$ still exhibits significant photocurrent. The calculated responsivity R and specific detectivity D^* related to optical density are negatively correlated with radiation intensity (Fig. 4b). Under 0.15 mW cm^{-2} irradiation, the calculated D^* and R values are 3.91×10^8 Jones and 0.99 μA W^{-1}, respectively, which were comparable to some reported lead-free perovskites (Table 1).[35,36] In addition, the $(4BrPEA)_3BiI_6$ device shows a fast rise/decay time of 29/

30 ms at 405 nm (Fig. 4c), which is superior to some reported lead-free perovskite photodetectors (Table 1).

Self-powered polarization-sensitive photodetection

Polar hybrid perovskites have also shown great potential in self-powered photodetection based on the BPVE.[40,41] The inherent polar structure drives us to further explore the BPVE behavior based on single crystal devices. Fig. 5a shows the current–voltage (I–V) photocurrent curves measured along the c-axis and a-axis (P = 2.94 mW cm^{-2}). The I–V curve on the c-axis shows obvious short-circuit current (I_{sc} = −1.3 pA) and open circuit voltage (V_{oc} = 1.45 V), while the current curve on the a-axis almost passes through the origin. The I–t curve measured along the c-axis under 0 V shows that the photocurrent increases sharply under illumination, and the I_{ph}/I_{dark} ratio is about 50 (Fig. 5b) (P = 4.04 mW cm^{-2}). The value of V_{oc} is larger than many Pb-based hybrid perovskites, such as $(BPA)_2PbBr_4$ (V_{oc} = 0.85 V) and $(BA)_2(FA)Pb_2I_7$ (V_{oc} = 0.3 V).[16,17]

The 2D $(4BrPEA)_3BiI_6$ perovskite structure has inherent structural anisotropy and can be used for polarization-sensitive photosensitive detection. Therefore, based on excellent BPVE activity, we further investigated the self-powered polarization-sensitive photoresponse of $(4BrPEA)_3BiI_6$. A 405 nm LED is used as the light source, ordinary light is converted into line-

Table 1 Summary of the reported lead-free perovskite photodetectors

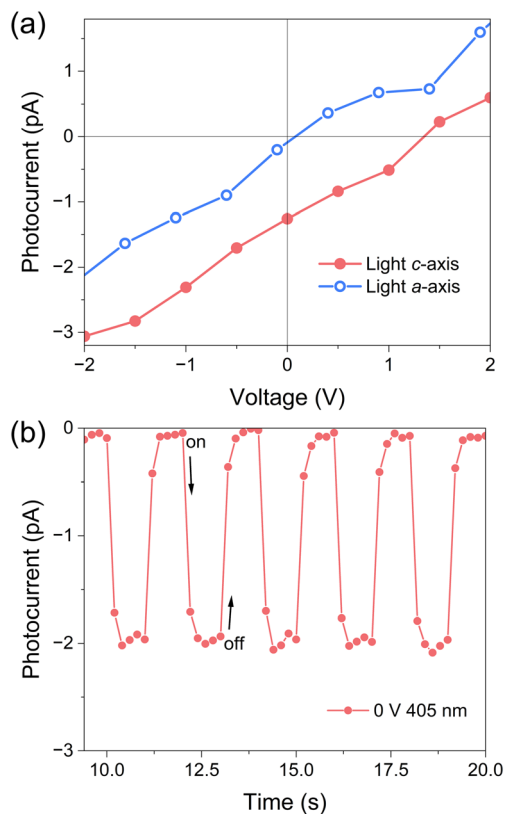| Compound	D^* (Jones)	R (A W^{-1})	Rise/decay time (ms)	Ref.
$Cs_3Bi_2I_9$	1.2×10^{10}	0.59 μ	88.66/109.3	35
$MA_3Bi_2I_9$	9.23×10^{11}	1.9 m	26.81/41.98	37
$HDABiI_5$	5.3×10^8	6.8 m	52/35	23
$Cs_3Bi_2I_6Br_3$	4.60×10^{11}	15 m	40.7/27.1	38
$AG_3Bi_2I_9$	8.8×10^{10}	14.8 m	0.152/0.187	39
$CsSnI_3$	3.85×10^5	54 m	83.8/243.4	36
$(4BrPEA)_3BiI_6$	3.91×10^8	0.99 μ	29/30	This work

Fig. 5 (a) *I–V* photocurrent curves measured along the *c*-axis and *a*-axis. (b) The *I–t* curve measured along the *c*-axis under 0 V bias.

arly polarized light through a polarizer, and the angle of LPL is controlled through a 1/2 wave plate (Fig. 6a) inside the *bc*-plane. The initial polarization angle (defined as 0°) of LPL is parallel to the *b*-axis. As shown in Fig. 6a, when the polarization angle of LPL is parallel to the *b*-axis, the photocurrent reaches its minimum value (I_{valley}). The value of photocurrent varies with the polarization angle, and when the LPL angle is parallel to the *c* direction, the maximum photocurrent value (I_{peak}) can be obtained. The polar coordination plot of the photocurrent and the polarization angle shows a clear double-lobed shape, and the calculated photocurrent anisotropy ratio ω (I_{peak}/I_{valley}) is 2.16. The *I–t* curve under pulsed light shows a clear polarization angle dependence, which proves the reproducibility and stability of the detector. Fig. 6e summarizes the performance of the reported perovskite and lead-based perovskite polarization-sensitive single crystal detectors.[17,23,42–47] The ω value of $(4BrPEA)_3BiI_6$ exceeds that of many lead-free perovskites and is even comparable to Pb-based perovskites.

The polarization-dependent photocurrent measured at 10 V bias is shown in Fig. S5,† and the photocurrent displays a small ω value of 1.05. This result demonstrates the enormous potential of BPVE-enhanced self-powered LPL detectors. The large ω value of $(4BrPEA)_3BiI_6$ at 0 V can be attributed to the angle dependence of the BPVE, which can be expressed as

$$J_z = I\beta_{31} \sin^2(\theta) + I\beta_{33} \cos^2(\theta)$$

where *I* is the light intensity, θ is the angle between the LPL polarization plane and the *z* axis (polar axis), and β_{31} and β_{33}
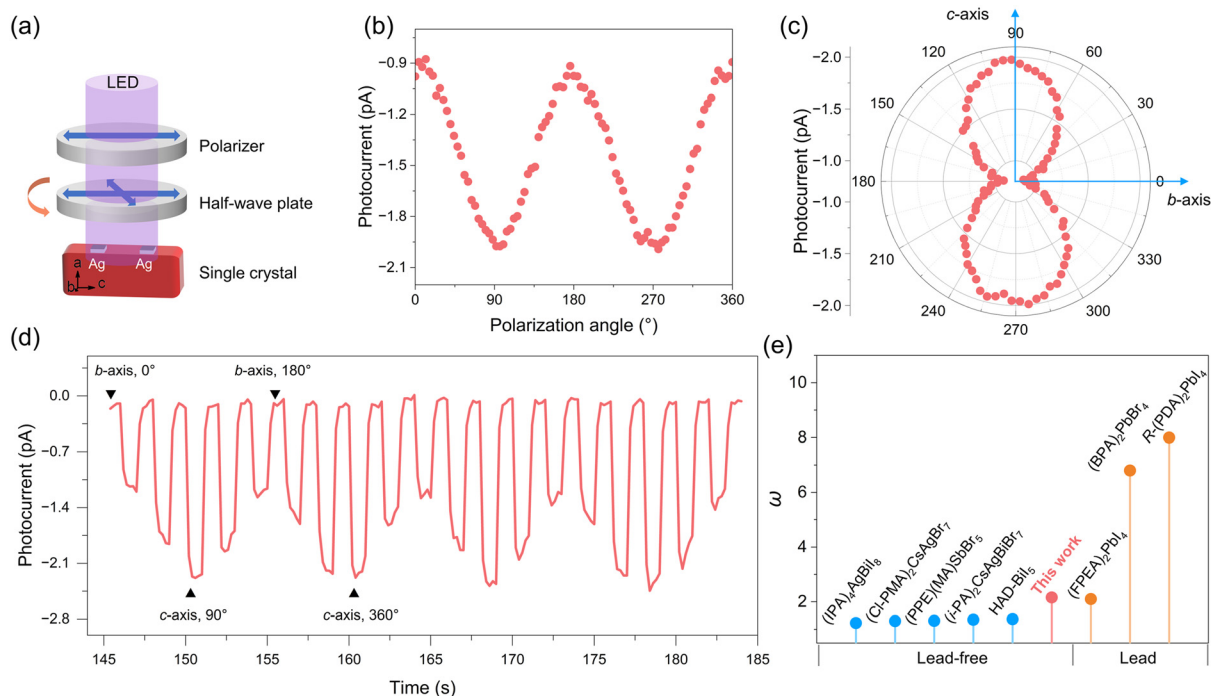
Fig. 6 (a) Schematic diagram of the polarization-sensitive photodetection device. (b) Angle-dependent photocurrent measured under 0 V bias. (c) Polar plots of the angle-dependent photocurrents measured under 0 V bias. (d) Angle-dependent *I–t* measurements at 405 nm pulsed light. (e) Comparison of the ω values for 2D perovskite photodetectors.

This journal is © the Partner Organisations 2024

Inorg. Chem. Front., 2024, **11**, 4611–4618 | **4615**

are the bulk photovoltaic coefficients.[48–51] Weak coupling occurs when the direction of LPL is perpendicular to the polar axis (c-axis), resulting in a low I_{valley}. While strong coupling occurs when the LPL is parallel to the polar axis, which promotes carrier separation, resulting in a large I_{peak} and ultimately highly sensitive polarization-sensitive detection.

Conclusions

In summary, by reasonably reducing the occupancy rate of Bi^{3+} on the 2D layer, we successfully obtained the first 2D polar Bi-based perovskite $(4BrPEA)_3BiI_6$ with an A_2PbX_4-like structure. $(4BrPEA)_3BiI_6$ single crystal devices exhibit photocurrent anisotropy ω values (2.16) comparable to Pb-based perovskite devices. This work provides an effective approach for the targeted design of green, lead-free, high-performance, 2D polarization-sensitive perovskites. At the same time, the narrow bandgap, low toxicity, high chemical stability, and excellent self-powered photodetection performance of $(4BrPEA)_3BiI_6$ also show its great application potential in solar cells and other photovoltaic conversion devices.

Experimental

Chemicals

Bismuth trioxide (Bi_2O_3, 99.0%,), 4-bromophenethylamine (4BrPEA, 98%), hypophosphorous acid (H_3PO_2, AR, 50 wt% in H_2O), and hydroiodic acid (HI, AR, 55.0–58%, contains ≤1.5% H_3PO_2 as a stabilizer) were all commercially obtained without further purification.

Synthesis of $(4BrPEA)_3BiI_6$

Bi_2O_3 (0.233 g, 0.5 mmol) was dissolved in 57% hydroiodic (HI) solution (100 mL) and then H_3PO_2 (5 mL) and 4BrPEA (0.600 g, 3 mmol) were slowly added dropwise. The mixture was stirred continuously at 373 K for 30 minutes until the precipitate was completely dissolved to give a clear red solution. Slowly cooling the red solution at a rate of 5 K day^{-1} from 373 K to 298 K resulted in the formation of dark red plate-shaped crystals of $(4BrPEA)_3BiI_6$.

Device fabrication

The surfaces of the single crystal were coated with silver paste along the different axes. The effective area of the crystal device was determined to be 1×0.3 mm^2 by the Phenix MC-D310U high-definition digital camera.

Photocurrent measurement

The photocurrent was measured using a PDA FS380 (Primarius) source meter. The 405 nm LED was obtained from Thorlabs. The polarizer (Glan–Taylor prism) converted the LED laser beam into polarized light, and the polarization angle of the polarized light was then adjusted by a half-wave plate. The state of the polarization state of linearly polarized

light was calibrated by a polarimeter system (PAX1000). The light intensity was measured using a digital console with a photodiode sensor (PM120VA, Thorlabs).

Author contributions

C.-D. L. performed most of the experiments and wrote the original manuscript. C.-C. F. and B.-D. L. participated in the writing and revision of the manuscript. W. Z. was responsible for funding acquisition, supervision, writing review, and editing. All authors discussed the results and commented on the manuscript.

Conflicts of interest

There are no conflicts to declare.

Acknowledgements

References

1 A. Kojima, K. Teshima, Y. Shirai and T. Miyasaka, Organometal Halide Perovskites as Visible-Light Sensitizers for Photovoltaic Cells, *J. Am. Chem. Soc.*, 2009, **131**, 6050–6051.

2 N. Wang, L. Cheng, R. Ge, S. Zhang, Y. Miao, W. Zou, C. Yi, Y. Sun, Y. Cao, R. Yang, Y. Wei, Q. Guo, Y. Ke, M. Yu, Y. Jin, Y. Liu, Q. Ding, D. Di, L. Yang, G. Xing, H. Tian, C. Jin, F. Gao, R. H. Friend, J. Wang and W. Huang, Perovskite light-emitting diodes based on solution-processed self-organized multiple quantum wells, *Nat. Photonics*, 2016, **10**, 699–704.

3 C. C. Stoumpos, C. D. Malliakas and M. G. Kanatzidis, Semiconducting tin and lead iodide perovskites with organic cations: phase transitions, high mobilities, and near-infrared photoluminescent properties, *Inorg. Chem.*, 2013, **52**, 9019–9038.

4 C.-Q. Jing, C.-Y. Chai, X.-B. Han, C.-D. Liu, W. Wang, T.-Y. Ju, J.-M. Zhang, M.-L. Jin, Q. Ye and W. Zhang, Sensing polarized light via switchable Rashba-Dresselhaus spin splitting in a ferroelectric semiconductor, *Matter*, 2024, **7**, 991–1001.

5 C.-C. Fan, X.-B. Han, B.-D. Liang, C. Shi, L.-P. Miao, C.-Y. Chai, C.-D. Liu, Q. Ye and W. Zhang, Chiral Rashba Ferroelectrics for Circularly Polarized Light Detection, *Adv. Mater.*, 2022, **34**, 2204119.

6 W. Q. Liao, Y. Zhang, C. L. Hu, J. G. Mao, H. Y. Ye, P. F. Li, S. D. Huang and R. G. Xiong, A lead-halide perovskite

4616 | *Inorg. Chem. Front.*, 2024, **11**, 4611–4618

This journal is © the Partner Organisations 2024

molecular ferroelectric semiconductor, *Nat. Commun.*, 2015, **6**, 7338.

7 I. H. Park, K. C. Kwon, Z. Zhu, X. Wu, R. Li, Q. H. Xu and K. P. Loh, Self-Powered Photodetector Using Two-Dimensional Ferroelectric Dion-Jacobson Hybrid Perovskites, *J. Am. Chem. Soc.*, 2020, **142**, 18592–18598.

8 C.-C. Fan, B.-D. Liang, C.-D. Liu, C.-Y. Chai, X.-B. Han and W. Zhang, Stable organic lead iodides with three-dimensional crystallographic and electronic structures showing high photoresponse, *Inorg. Chem. Front.*, 2022, **9**, 6404–6411.

9 D. Shi, V. Adinolfi, R. Comin, M. Yuan, E. Alarousu, A. Buin, Y. Chen, S. Hoogland, A. Rothenberger, K. Katsiev, Y. Losovyj, X. Zhang, P. A. Dowben, O. F. Mohammed, E. H. Sargent and O. M. Bakr, Low trap-state density and long carrier diffusion in organolead trihalide perovskite single crystals, *Science*, 2015, **347**, 519–522.

10 B. D. Liang, C. C. Fan, C. D. Liu, C. Y. Chai, X. B. Han and W. Zhang, Near-room-temperature martensitic actuation profited from one-dimensional hybrid perovskite structure, *Nat. Commun.*, 2022, **13**, 6599.

11 W. Wang, C. D. Liu, C. C. Fan, X. B. Fu, C. Q. Jing, M. L. Jin, Y. M. You and W. Zhang, Rational Design of 2D Metal Halide Perovskites with Low Congruent Melting Temperature and Large Melt-Processable Window, *J. Am. Chem. Soc.*, 2024, **146**, 9272–9284.

12 B. Vargas, G. Rodríguez-López and D. Solis-Ibarra, The Emergence of Halide Layered Double Perovskites, *ACS Energy Lett.*, 2020, **5**, 3591–3608.

13 T. Li, S. Luo, X. Wang and L. Zhang, Alternative Lone-Pair ns^2-Cation-Based Semiconductors beyond Lead Halide Perovskites for Optoelectronic Applications, *Adv. Mater.*, 2021, **33**, 2008574.

14 Y. Zhang, Y. Ma, Y. Wang, X. Zhang, C. Zuo, L. Shen and L. Ding, Lead-Free Perovskite Photodetectors: Progress, Challenges, and Opportunities, *Adv. Mater.*, 2021, **33**, 2006691.

15 L. Mao, C. C. Stoumpos and M. G. Kanatzidis, Two-Dimensional Hybrid Halide Perovskites: Principles and Promises, *J. Am. Chem. Soc.*, 2018, **141**, 1171–1190.

16 Z. Xu, X. Dong, L. Wang, H. Wu, Y. Liu, J. Luo, M. Hong and L. Li, Precisely Tailoring a FAPbI$_3$-Derived Ferroelectric for Sensitive Self-Driven Broad-Spectrum Polarized Photodetection, *J. Am. Chem. Soc.*, 2023, **145**, 1524–1529.

17 C. Ji, D. Dey, Y. Peng, X. Liu, L. Li and J. Luo, Ferroelectricity-Driven Self-Powered Ultraviolet Photodetection with Strong Polarization Sensitivity in a Two-Dimensional Halide Hybrid Perovskite, *Angew. Chem., Int. Ed.*, 2020, **59**, 18933–18937.

18 J. Ma, C. Fang, L. Liang, H. Wang and D. Li, Full-Stokes Polarimeter Based on Chiral Perovskites with Chirality and Large Optical Anisotropy, *Small*, 2021, **17**, 2103855.

19 L. Li, L. Jin, Y. Zhou, J. Li, J. Ma, S. Wang, W. Li and D. Li, Filterless Polarization-Sensitive 2D Perovskite Narrowband Photodetectors, *Adv. Opt. Mater.*, 2019, **7**, 1900988.

20 A. J. Dennington and M. T. Weller, Synthesis, structure and optoelectronic properties of hybrid iodobismuthate & iodoantimonate semiconducting materials, *Dalton Trans.*, 2018, **47**, 3469–3484.

21 L. Yao, Z. Zeng, C. Cai, P. Xu, H. Gu, L. Gao, J. Han, X. Zhang, X. Wang, X. Wang, A. Pan, J. Wang, W. Liang, S. Liu, C. Chen and J. Tang, Strong Second- and Third-Harmonic Generation in 1D Chiral Hybrid Bismuth Halides, *J. Am. Chem. Soc.*, 2021, **143**, 16095–16104.

22 R. Jakubas, M. Rok, K. Mencel, G. Bator and A. Piecha-Bisiorek, Correlation between crystal structures and polar (ferroelectric) properties of hybrids of haloantimonates(III) and halobismuthates(III), *Inorg. Chem. Front.*, 2020, **7**, 2107–2128.

23 C.-D. Liu, C.-C. Fan, B.-D. Liang, C.-Y. Chai, C.-Q. Jing, X.-B. Han and W. Zhang, Spectrally Selective Polarization-Sensitive Photodetection Based on a 1D Lead-Free Hybrid Perovskite Ferroelectric, *ACS Mater. Lett.*, 2023, **5**, 1974–1981.

24 L. Peedikakkandy, S. Chatterjee and A. J. Pal, Bandgap Engineering and Efficient Conversion of a Ternary Perovskite (Cs$_3$Bi$_2$I$_9$) to a Double Perovskite (Cs$_2$NaBiI$_6$) with the Aid of Alkali Metal Sulfide, *J. Phys. Chem. C*, 2020, **124**, 10878–10886.

25 D. B. Mitzi, Organic–Inorganic Perovskites Containing Trivalent Metal Halide Layers: The Templating Influence of the Organic Cation Layer, *Inorg. Chem.*, 2000, **39**, 6107–6113.

26 M. Li, H. Li, W. Li, B. Li, T. Lu, X. Feng, C. Guo, H. Zhang, H. Wei and B. Yang, Oriented 2D Perovskite Wafers for Anisotropic X-ray Detection through a Fast Tableting Strategy, *Adv. Mater.*, 2022, **34**, 2108020.

27 H. Peng, Q. Liu, Y. Z. Lu, S. J. Yang, J. C. Qi, X. G. Chen and W. Q. Liao, A chiral two-dimensional perovskite-like lead-free bismuth(III) iodide hybrid with high phase transition temperature, *Chem. Commun.*, 2023, **59**, 10295–10298.

28 T. Schmitt, S. Bourelle, N. Tye, G. Soavi, A. D. Bond, S. Feldmann, B. Traore, C. Katan, J. Even, S. E. Dutton and F. Deschler, Control of Crystal Symmetry Breaking with Halogen-Substituted Benzylammonium in Layered Hybrid Metal-Halide Perovskites, *J. Am. Chem. Soc.*, 2020, **142**, 5060–5067.

29 D. B. Straus, N. Iotov, M. R. Gau, Q. Zhao, P. J. Carroll and C. R. Kagan, Longer Cations Increase Energetic Disorder in Excitonic 2D Hybrid Perovskites, *J. Phys. Chem. Lett.*, 2019, **10**, 1198–1205.

30 L. Mao, W. Ke, L. Pedesseau, Y. Wu, C. Katan, J. Even, M. R. Wasielewski, C. C. Stoumpos and M. G. Kanatzidis, Hybrid Dion–Jacobson 2D Lead Iodide Perovskites, *J. Am. Chem. Soc.*, 2018, **140**, 3775–3783.

31 C. C. Stoumpos, D. H. Cao, D. J. Clark, J. Young, J. M. Rondinelli, J. I. Jang, J. T. Hupp and M. G. Kanatzidis, Ruddlesden–Popper Hybrid Lead Iodide Perovskite 2D Homologous Semiconductors, *Chem. Mater.*, 2016, **28**, 2852–2867.

This journal is © the Partner Organisations 2024

Inorg. Chem. Front., 2024, **11**, 4611–4618 | **4617**

32 J. Y. Kim, J. W. Lee, H. S. Jung, H. Shin and N. G. Park, High-Efficiency Perovskite Solar Cells, *Chem. Rev.*, 2020, **120**, 7867–7918.

33 H. Y. Zhang, Z. Wei, P. F. Li, Y. Y. Tang, W. Q. Liao, H. Y. Ye, H. Cai and R. G. Xiong, The Narrowest Band Gap Ever Observed in Molecular Ferroelectrics: Hexane-1,6-diammonium Pentaiododobismuth(III), *Angew. Chem., Int. Ed.*, 2018, **57**, 526–530.

34 A. Maiti and A. J. Pal, Effect of Cation Occupancy Ordering in Double Perovskites To Overcome Hurdles in Carrier Transport: $Cs_2AgBiBr_6$ as a Case Study, *J. Phys. Chem. C*, 2021, **125**, 16324–16333.

35 A. A. Hussain, Constructing Caesium-Based Lead-Free Perovskite Photodetector Enabling Self-Powered Operation with Extended Spectral Response, *ACS Appl. Mater. Interfaces*, 2020, **12**, 46317–46329.

36 M. Han, J. Sun, M. Peng, N. Han, Z. Chen, D. Liu, Y. Guo, S. Zhao, C. Shan, T. Xu, X. Hao, W. Hu and Z.-X. Yang, Controllable Growth of Lead-Free All-Inorganic Perovskite Nanowire Array with Fast and Stable Near-Infrared Photodetection, *J. Phys. Chem. C*, 2019, **123**, 17566–17573.

37 A. A. Hussain, A. K. Rana and M. Ranjan, Air-stable lead-free hybrid perovskite employing self-powered photodetection with an electron/hole-conductor-free device geometry, *Nanoscale*, 2019, **11**, 1217–1227.

38 D. Liu, B. B. Yu, M. Liao, Z. Jin, L. Zhou, X. Zhang, F. Wang, H. He, T. Gatti and Z. He, Self-Powered and Broadband Lead-Free Inorganic Perovskite Photodetector with High Stability, *ACS Appl. Mater. Interfaces*, 2020, **12**, 30530–30537.

39 W. Zhang, Y. Sui, B. Kou, Y. Peng, Z. Wu and J. Luo, Large-Area Exfoliated Lead-Free Perovskite-Derivative Single-Crystalline Membrane for Flexible Low-Defect Photodetectors, *ACS Appl. Mater. Interfaces*, 2020, **12**, 9141–9149.

40 P.-J. Huang, K. Taniguchi and H. Miyasaka, Bulk Photovoltaic Effect in a Pair of Chiral-Polar Layered Perovskite-Type Lead Iodides Altered by Chirality of Organic Cations, *J. Am. Chem. Soc.*, 2019, **141**, 14520–14523.

41 P.-J. Huang, K. Taniguchi and H. Miyasaka, Crucial Contribution of Polarity for the Bulk Photovoltaic Effect in a Series of Noncentrosymmetric Two-Dimensional Organic–Inorganic Hybrid Perovskites, *Chem. Mater.*, 2022, **34**, 4428–4436.

42 Z. Li, Q. Chen, Z. Y. Wang, Y. P. Fan, T. T. Zhu, C. M. Ji, X. J. Kuang and J. H. Luo, Centimeter-size single crystal of a lead-free double perovskite for broad-spectrum polarization-sensitive detection, *J. Mater. Chem. C*, 2022, **10**, 18063–18068.

43 W. Wu, Z. Xu, Y. Yao, Y. Liu, G. Long, L. Li, M. Hong and J. Luo, Realization of In-Plane Polarized Light Detection Based on Bulk Photovoltaic Effect in A Polar van der Waals Crystal, *Small*, 2022, **18**, 2200011.

44 W. C. Zhang, M. C. Hong and J. H. Luo, Centimeter-Sized Single Crystal of a One-Dimensional Lead-Free Mixed-Cation Perovskite Ferroelectric for Highly Polarization Sensitive Photodetection, *J. Am. Chem. Soc.*, 2021, **143**, 16758–16767.

45 Y. Li, T. Yang, Z. Xu, X. Liu, X. Huang, S. Han, Y. Liu, M. Li, J. Luo and Z. Sun, Dimensional Reduction of $Cs_2AgBiBr_6$: A 2D Hybrid Double Perovskite with Strong Polarization Sensitivity, *Angew. Chem., Int. Ed.*, 2020, **59**, 3429–3433.

46 M. Li, S. Han, B. Teng, Y. Li, Y. Liu, X. Liu, J. Luo, M. Hong and Z. Sun, Minute-Scale Rapid Crystallization of a Highly Dichroic 2D Hybrid Perovskite Crystal toward Efficient Polarization–Sensitive Photodetector, *Adv. Opt. Mater.*, 2020, **8**, 2000149.

47 B.-D. Liang, C.-C. Fan, C.-D. Liu, T.-Y. Ju, C.-Y. Chai, X.-B. Han and W. Zhang, Large in-plane anisotropic 2D perovskites toward highly linear polarized light responses, *Inorg. Chem. Front.*, 2023, **10**, 5035–5043.

48 M. M. Yang and M. Alexe, Light-Induced Reversible Control of Ferroelectric Polarization in $BiFeO_3$, *Adv. Mater.*, 2018, **30**, 1704908.

49 W. T. H. Koch, R. Munser, W. Ruppel and P. Würfel, Anomalous photovoltage in $BaTiO_3$, *Ferroelectrics*, 1976, **13**, 305–307.

50 T. Choi, S. Lee, Y. J. Choi, V. Kiryukhin and S.-W. Cheong, Switchable Ferroelectric Diode and Photovoltaic Effect in $BiFeO_3$, *Science*, 2009, **324**, 63–66.

51 M.-M. Yang, Z.-D. Luo, D. J. Kim and M. Alexe, Bulk photovoltaic effect in monodomain $BiFeO_3$ thin films, *Appl. Phys. Lett.*, 2017, **110**, 183902.

4618 | *Inorg. Chem. Front.*, 2024, **11**, 4611–4618

This journal is © the Partner Organisations 2024